THEORETICAL & APPLIED MECHANICS LETTERS **4**, 062002 (2014)

Meso-level simulation of gas hydrate dissociation in low-permeability sediments

Jianhong Zhang,[a] Chao Zhao, Zhongsheng Xiong
State Key Laboratory of Hydroscience and Engineering, Tsinghua University, Beijing 100084, China

(Received 17 March 2014; revised 23 June 2014; accepted 21 July 2014)

Abstract This paper presents a meso-level simulation of gas hydrate dissociation in low-permeability marine sediments. Interstitial pores are defined to describe fluid flow and particle movement. The proposed model couples multiphase fluid flow with particle movement to simulate the thermodynamics of gas hydrate dissociation triggered by sharp temperature rises. Hydrates respond quickly to temperature rise in low-permeability sediments. Dissociation causes pore pressure to rise rapidly to equilibrium then steadily increase above equilibrium pressure. Lower permeability sediment builds up greater excess pore pressure as the dissipation of pore pressure is constrained.

 [doi:10.1063/2.1406202]

Keywords gas hydrate dissociation, particle movements, pore pressure, discrete element model

Gas hydrates are solid, ice-like crystalline materials consisting of gas molecules, especially methane, trapped in a water lattice.[1–3] They exist in a natural form at low temperature and high pressure in permafrost regions onshore and in ocean basins offshore. However, the gas hydrates dissociate and produce gas and water when the ambient temperature rises or pressure decreases.[4] Since gas hydrate dissociation generates excess pore pressure that considerably decreases the strength of the soil,[5] the kinetics of gas hydrate formation and dissociation is of a particular concern to the petroleum industry for an evaluation of environmental hazards in deep offshore areas. For instance, many researchers have related submarine landslides to gas hydrate dissociation.[6–11]

Of particular interest to the problem of hydrate kinetics is the three-phase thermodynamic equilibrium of these compounds. Prediction of the fate and migration of gas hydrates in complex soil systems requires the influence of temperature, pressure, pore water chemistry, pore space or volume change, permeability of soils, and solubilities of fluids to all be considered. Much work has been done on the simulation of kinetics on hydrate formation and dissociation at the grain or pore scale and the macro scale with powerful numerical tools, including discrete element methods (DEM), finite element methods (FEM), and finite difference methods (FDM).[5,12–17]

This paper presents a theoretical study of the thermodynamic equilibrium of a gas hydrate in low permeability marine sediments. The kinetics of gas hydrate dissociation at the meso-scale is described in terms of particle movement, pore volume change, pressure change, and temperature change. A two-dimensional mathematical model for hydrate dissociation was derived with Par-

[a]Corresponding author. Email: cezhangjh@mail.tsinghua.edu.cn.

ticle Flow Code (PFC), considering two-phase gas and liquid flow, and interactions between the fluid and the sediment particle.

Theoretical model There is no model in PFC to describe the pores between particles and the fluid flow in pores. Therefore, in the present study, a pore is defined to be the space between contact particles, or the space between particles and its contact side walls. The sediment is considered to be composed of solid particles and pores. The pores are filled with liquid and gas bubbles resulting from hydrate dissociation.

The particles are assumed to be rigid circular disks with flexible point contacts. For the two-dimensional PFC,[18] the contact is defined as the tube channel shown in Fig. 1, linking two pores on either side of the contact and facilitating fluid flow between pores. The length of the tube channel, i.e., L in Fig. 2, equals to the distance between the centers of the two pores. The radius of the tube channel, r_{th}, is inversely proportional to the contact force, i.e., the greater the contact force, the smaller the tube channel. It has the form as $r_{\text{th}} = r_{\text{th0}}F_0/(F_0 + F_{\text{n}})$, where F_0 is a parameter defining the size of the tube channel, F_{n} is the contact force between particles, and r_{th0} is the initial radius when the contact force equals zero. The value of r_{th0} is equal to one-half of the radius of the smaller particle between of the two in contact,[16] having $r_{\text{th0}} = 0.5\min(r_1, r_2)$, where r_1, r_2 are the radii of the particles in contact.

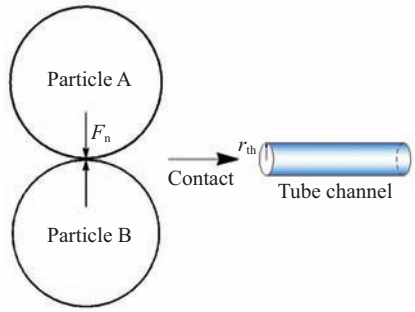

Fig. 1. Tube channel at a contact between particles.

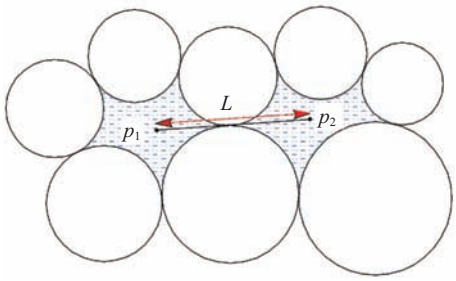

Fig. 2. Length of tube channel between two adjacent pores.

Interactions between particles result in merging or splitting of pores. These are characterized by the contact force between particles and the consequent induced particle movement. Figure 3 shows two pores formed by four contact particles. When the contact force between particles A and C decreases to zero, two pores on either side of the contact merge to one. Vice versa, one pore splits into two when the contact force between particles A and C is greater than zero.

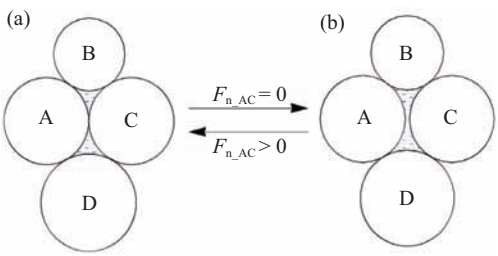

Fig. 3. (a) Split of a pore and (b) merging of pores.

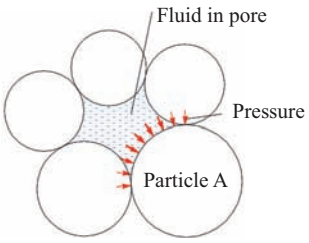

Fig. 4. Pore pressure on particle imposed by fluid in the pore.

The fluid in the sediment, that is, gas and water, shown in Fig. 4 is characterized by the pore pressure exerted on the surface of the particle. The force on the particle imposed by the fluid in the pore thus can be determined.

For simplification, the isolated gas bubble is assumed to be in the center of the pore and is surrounded by water. The gas pressure, p_g, equals the water pressure p_w, as shown in Fig. 5 ($p_g = p_w$). When fluid flows, it is assumed that water comes first out of a pore. Only when there is no water in the pore, can gas flow. The surface tension existing at gas-water interface is to be overcome to facilitate the gas flow out of the pore as $p_{lg} - p_{lw} \geqslant 2T_t \cos\theta / r_{th}$, where p_{1g} is the gas pressure when the pore is full of gas, p_{1w} is the water pressure, T_t is the surface tension on the gas-water interface, and θ is the wetting angle (Fig. 6).

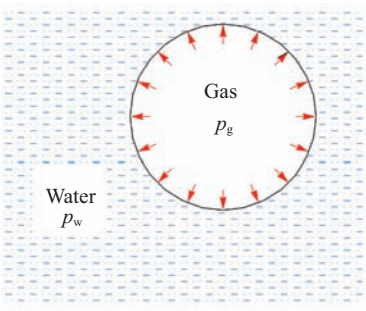

Fig. 5. Gas in a pore.

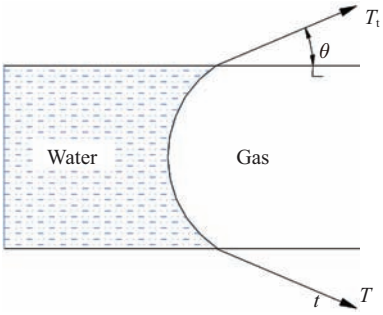

Fig. 6. Gas-water interface and wetting angle.

In meso-scale, the flow through pores is governed by Poiseuille's law. The discharge can be calculated in terms of laminar flow in tubes as[19] $q_{1-2} = \pi r_{th}^4 \Delta p/(8\mu L) = \pi r_{th}^4 (p_1 - p_2)\ /(8\mu L)$, where μ is the coefficient of dynamic viscosity of fluid, p_1 and p_2 are pressures in the two pores, and L is the length of the tube channel, as shown in Fig. 2. The fluid flow greatly depends on the properties of the fluid and the sediment matrix.

In order to facilitate the understanding of hydrate kinetics at a macro-scale, the coefficient of permeability is provided with Darcy's law. It can be determined through permeability test. In this study, a numerical simulation is carried out instead to obtain the coefficient of permeability.

The chemical formula of the hydrate is $CH_4{\cdot}5.75H_2O$. The dissociation of the hydrate can therefore be expressed as: $CH_4{\cdot}\ 5.75H_2O \rightarrow CH_4 \uparrow + 5.75H_2O$.

The gas hydrate dissociates only when the temperature is higher or the pressure is lower than the equilibrium values. The gas resulting from dissociation exists around the gas hydrate as illustrated in Fig. 7. Figure 8 shows the pressure–temperature equilibrium line that defines the state of the hydrate in the sediment. The gas hydrate is solid when the pressure–temperature data point is above the equilibrium line, and is dissociated when the data point falls below the line. The pressure on the line at the corresponding temperature is the equilibrium pressure.

The dissociation rate of the hydrate associated with change of pressure and/or temperature can be calculated from

$$\mathrm{d}n_h/\mathrm{d}t = -K_h A_h (f_{eq} - f), \tag{1}$$

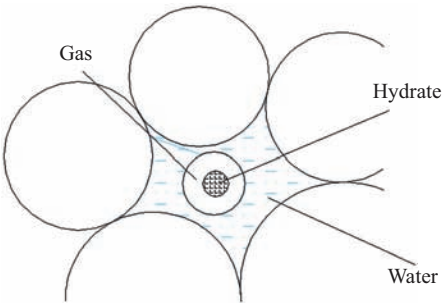

Fig. 7. Hydrate, gas, and water in a pore.

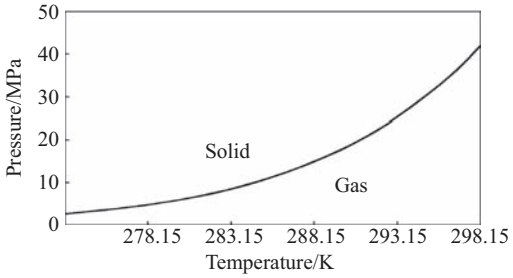

Fig. 8. Pressure–temperature equilibrium of hydrate with salinity of 3.5%.

where $\mathrm{d}n_\mathrm{h}/\mathrm{d}t$ is the dissociation rate of hydrate, A_h is the surface area of the solid hydrate particle, f_eq is the equilibrium fugacity and quantified by the equilibrium pressure for gas hydrate at certain temperature, f is and the current fugacity and quantified by the ambient pressure, and K_h is a function of Kelvin temperature (T)[20] as $K_\mathrm{h} = -\exp(25.54 - 9400/T)$.

Assuming the hydrate to be a sphere, its surface area is calculated from

$$A_\mathrm{h} = 4\pi r^2 = 4\pi\{[3/(4\pi)](n_\mathrm{h}M_\mathrm{h}/\rho_\mathrm{h})\}^{2/3}, \tag{2}$$

where n_h is the number of molecular of hydrate in the pore, $M_\mathrm{h} = 0.1195$ kg/mol is the molecular weight of the hydrate, and $\rho_\mathrm{h} = 920$ kg/m^3 is the density of the hydrate. Substituting Eq. (2) in Eq. (1), it becomes $\mathrm{d}n_\mathrm{h}/\mathrm{d}t = -K_\mathrm{h}A_\mathrm{h}\Delta p$, where Δp is the difference between ambient pressure and equilibrium pressure.

Complex interactions between the fluid and the sediment particle are incorporated. High excess pore pressure will build up during methane hydrate dissociation in low permeability sediment where pores are not well connected. The pore pressure imposed on particles by fluid will stimulate particle movement, which directly alters the pore volume and may result in the merging or splitting of pores. This in turn may change the pressure of the fluid and eventually influence the movement of particles. The ideal gas state equation used to estimate the pore pressure is

$$p_\mathrm{g}V_\mathrm{g} = n_\mathrm{g}RT, \tag{3}$$

where p_g is the pressure of methane, V_g is the volume of methane gas, n_g is number of molecular of the methane hydrate in the pore, and R is a constant. Neglecting the compression of water, the total gas volume change is

$$\mathrm{d}V_\mathrm{g} = \mathrm{d}V_\mathrm{diss} + \mathrm{d}V_\mathrm{flow} + \mathrm{d}V_\mathrm{motion}, \tag{4}$$

where $\mathrm{d}V_\mathrm{g}$ is the total volume change of gas, $\mathrm{d}V_\mathrm{diss}$ is the gas volume change from hydrate dissociation, $\mathrm{d}V_\mathrm{flow}$ is the gas volume change due to fluid flow, and $\mathrm{d}V_\mathrm{motion}$ is the gas volume change due to particle movement. Combining Eq. (4) with Eq.(3) gives $(p_\mathrm{g} + \mathrm{d}p_\mathrm{g})(V_\mathrm{g} + \mathrm{d}V_\mathrm{diss} + \mathrm{d}V_\mathrm{flow} + \mathrm{d}V_\mathrm{motion}) = (n_\mathrm{g} + \mathrm{d}n_\mathrm{g\_diss} + \mathrm{d}n_\mathrm{g\_flow})RT$, where $\mathrm{d}p_\mathrm{g}$ is the pressure change of methane gas, $\mathrm{d}n_\mathrm{g\_diss}$

is the change of gas molecular from hydrate dissociation, and dn_{g_flow} is the change of gas molecular due to fluid flow.

The proposed model is written in FISH language and executed by PFC2D software, using the time-domain analysis method. It was verified by the authors through one-dimensional steady and unsteady seepage simulation with no gas hydrate

Gas hydrate dissociation in low-permeability sediments Consider the uniform sediment sample illustrated in Fig. 9. Particles are shown in orange; pores are shown in gray. The volume saturation of gas hydrate in the pore space is 15%. The size of sample is 25 mm × 25 mm. The permeability coefficient of the sediment is 2.86×10^{-10} m/s.[21] The radius of the particles ranges between 0.44 mm and 0.66 mm, initial pore ratio is $e = 0.15$, initial number of pores is 694, and number of particles is 554. The parameters used in the model are listed in Table 1. The bottom and both sides of the sample are impermeable and unmovable. The top of the sample is set to the drained condition and constant pore pressure is applied. The sample has been consolidated under a confined pressure of 1 MPa.

Table 1. Parameters used in simulation.

Parameter	Normal stiffness/(N·m^{-1})	Tangential stiffness/(N·m^{-1})	Friction coefficient	Density/(kg·m^{-3})	Permeability coefficient/(m·s^{-1})
Contact between particles	1.0×10^8	1.0×10^8	0.25	2.65×10^3	2.86×10^{-10}

The pores were assumed to be initially filled with water, with no free gas. The bulk modulus of water is high, i.e, 2.2 GPa, and the time step needed to be small to ensure computational stability. In this study, the time step was 1×10^{-8} s to 1×10^{-7} s. The calculation was time-consuming.

The temperature was assumed to rise abruptly from 2°C to 5°C to trigger hydrate dissociation in the sample. The ambient pressure was set at 3.6 MPa. The hydrate kinetics was simulated, for which the pore pressure, hydrate content, pore number, radius of the pore channel, and gas and water contents were calculated.

Figure 10 shows the relationship between pore pressure and percentage of hydrate dissociation. The induced sharp rise, fluctuating state, and steady state of the pore pressure are shown as A, B, and C in Fig. 10.

Figure 10 shows that between 0 s to 0.005 s, the pore pressure rose rapidly from the ambient pressure of 3.6 MPa to 4.84 MP which is the equilibrium pressure at the temperature of 283.15 K.

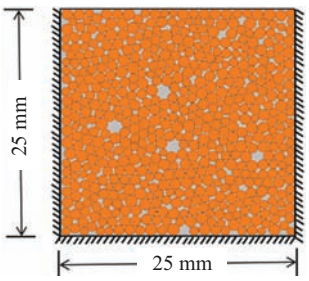

Fig. 9. Model sample to simulate dissociation.

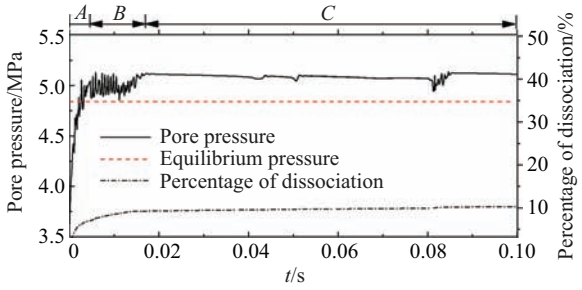

Fig. 10. Pore pressure during hydrate dissociation.

The hydrate dissociation was simulated to rapidly reach 5%, indicating that the hydrate immediately responds to the rise in temperature, dissociating and increasing the pore pressure.

When the pore pressure fluctuates up to 5.13 MPa between 0.005 s and 0.018 s, hydrate dissociation continues to rise to 9.5%. Although the pore pressure exceeds the equilibrium value, the dissociation is not constrained. This may be attributed to the oscillating motion of particles stimulated by the excess pore pressure (Fig. 11). Movement of the particles causes the pressure in some pores to fall below the equilibrium value, which then enables dissociation. This kind of disturbance by particle movement is gradually suppressed, leading to stabilized pore pressures. The dissociation is then suspended and a new pressure–temperature equilibrium is reached. By the end of the computation, about 10 percent of the hydrate was predicted to have dissociated.

The permeability is to a great extent related to the properties of the sediment and the contents of the gas hydrate. These effects were examined by a parametric study with different coefficients of permeability of the sediment. The calculation condition was identical to the previous simulation. Figure 12 shows the calculated maximum pore pressure in samples with different permeability coefficients. It indicates that greater excess pore pressures were exhibited in sediments with lower permeability, where the pores were more confined. Higher permeability, where pores are better connected, facilitates pore pressure dissipation.

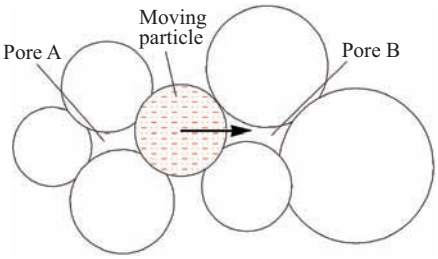

Fig. 11. Particle movement and pore pressure change.

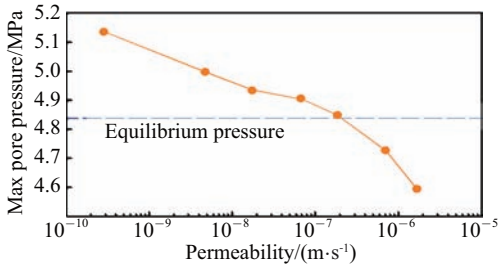

Fig. 12. Relationship between permeability and maximum pore pressure.

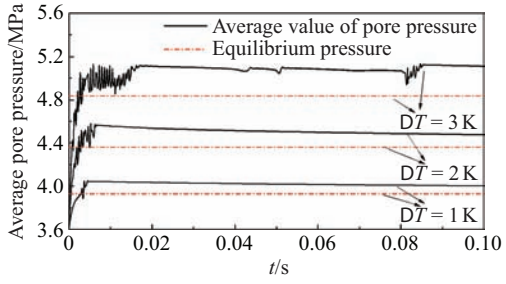

Fig. 13. Excess pore pressures with different temperature variation.

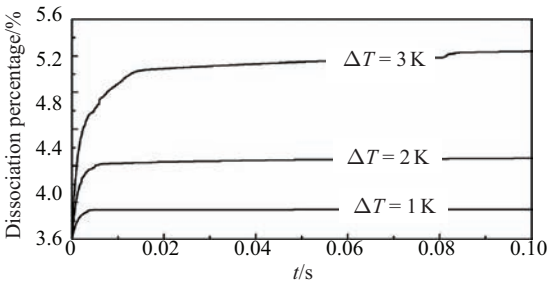

Fig. 14. Hydrate dissociation at different temperature rise.

Different temperature increments $\Delta T = 1$ K, 2 K, and 3 K from the initial value were applied on the same sample to study its effect on hydrate dissociation. Figure 13 compares the calculated average pore pressure in the sample due to hydrate dissociation. The pore pressure induced by dissociation rose quickly, exceeding the equilibrium pressure in all cases. The response was more significant with greater temperature increments, and the total percentage dissociation also

increased with greater temperature increments, i.e., 10%, 4%, and 1.8% for $\Delta T = 3$ K, 2 K, and 1 K (as shown in Fig. 14).

Conclusions This paper describes interactions between gas, water, and hydrate by defining the pores and the fluid flow in the pores using the discrete element model with PFC code. The model coupled hydrate dissociation, multiphase fluid flow and particle movement. The following conclusions were drawn.

In low permeability sediment, hydrate responds quickly to rise in temperature. The pore pressure induced by dissociation rose rapidly to the equilibrium pressure, then steadily increased to a value greater than the equilibrium pressure. This phase was associated with particle movement.

Greater excess pore pressure occurred in lower permeability sediment, as the pores were more confined and pore pressure dissipation was restricted. Temperature rise played a very important role in hydrate dissociation and excess pore pressure increase

This work was supported by the National Basic Research Program of China (2013CB035902), the National Natural Science Foundation of China (51038007), and the State Key Laboratory of Hydroscience and Engineering Project (2013-KY-04 and 2014-KY-03).

1. I. U. F. Makogon. Hydrates of Natural Gas. Pennwell, Tulsa (1985).
2. E. D. Sloan, K. Carolyn. Clathrate Hydrates of Natural Gases. CRC Press , Boca Raton (2007).
3. E. D. Sloan. Fundamental principles and applications of natural gas hydrates. *Nature* **426**, 353–363 (2003).
4. J. Louis, A. C. Briaud. Hydrate melting in soil around hot conductor. *Journal of Geotechnical and Geoenvironmental Engineering* **123**, 645–653 (1997).
5. N. Sultan, P. Cochonat, P. J. Foucher. Effect of gas hydrates melting on seafloor slope instability. *Marine Geology* **213**, 379–401 (2004).
6. N. W. Driscoll, J. K. Weissel, J. A. Goff. Potential for large-scale submarine slope failure and tsunami generation along the us mid-atlantic coast. *Geology* **28**, 407–410 (2000).
7. D. E. Smith, S. Shi, R. Cullingford. The holocene Storegga slide tsunami in the united kingdom. *Quaternary Science Reviews* **23**, 2291–2321 (2004).
8. M. Vanneste, J. Mienert, S. Bünz. The hinlopen slide: a giant, submarine slope failure on the northern svalbard margin, arctic ocean. *Earth and Planetary Science Letters* **245**, 373–388 (2006).
9. Kimoto, Sayuri. A chemo-thermo-mechanically coupled numerical simulation of the subsurface ground deformations due to methane hydrate dissociation. *Computers and Geotechnics* **34**, 216–228 (2007).
10. L. Li, X. H. Lei, X. Zhang, et al. Gas hydrate and associated free gas in the Dongsha area of northern south china sea. *Marine and Petroleum Geology* **39**, 92–101 (2013).
11. C. Zhao, W. Z. Zhang, J. H. Zhang, et al. Modelling techniques of submarine landslide in centrifuge. 4th International Symposium on Geotechnical Safety and Risk. Hong Kong, 235–238 (2013).
12. W. Y. Xu, L. N. Germanovich. Excess pore pressure resulting from methane hydrate dissociation in marine sediments: a theoretical approach. *Journal of Geophysical Research: Solid Earth* **111**, 1978–2012 (2006).
13. T. H. Kwon, G. C. Cho, J. C. Santamarina. Gas hydrate dissociation in sediments: pressure-temperature evolution. *Geochemistry Geophysics Geosystems* **9**, Q3019 (2008).
14. K. Jain, R. Juanes. Preferential mode of gas invasion in sediments: grain-scale mechanistic model of coupled multiphase fluid flow and sediment mechanics. *Journal of Geophysical Research: Solid Earth* **114**, (2009).
15. R. Holtzman, R. Juanes. Thermodynamic and hydrodynamic constraints on overpressure caused by hydrate dissociation: a pore-scale model. *Geophysical Research Letters* **38**, L14308 (2011).
16. J. Jang, J. C. Santamarina. Recoverable gas from hydrate-bearing sediments: pore network model simulation and macroscale analyses. *Journal of Geophysical Research: Solid Earth* (1978–2012) **116**, (2011).
17. I. N. Tsimpanogiannis, N. Ioannis, P. C. Lichtner. Gas saturation resulting from methane hydrate dissociation in a porous medium: comparison between analytical and pore-network results. *Journal of Physical Chemistry C* **117**, 11104–11116 (2013).
18. Itasca Consulting Group. Particle flow code in 2 dimensions user's manual. Minneapolis (2008).
19. S. P. Sutera, R. Skalak. The history of poiseuille law. *Annual Review of Fluid Mechanics* **25**, 1–19 (1993).
20. H. C. Kim, P. R. Bishnoi, R. A. Heidemann, et al. Kinetics of methane hydrate decomposition. *Chemical Engineering Science* **42**, 1645–1653 (1987).
21. W. J. Winters, I. A. Pecher, W. F. Waite, et al. Physical properties and rock physics models of sediment containing natural and laboratory-formed methane gas hydrate. *American Mineralogist* **89**, 1221–1227 (2004).